19th Brazilian Congress of Thermal Sciences and Engineering
November 6th–10th, 2022, Bento Gonçalves - RS - Brazil

ENC-2022-0268
NEW APPROACHES IN THE STUDY OF WATER-OIL FLOW IN A PDMS-BASED POROUS MEDIA MICROMODEL

Jesús Daniel Fernández
Clarice de Amorim
Amanda C. S. N. Pessoa
Jorge Avendaño
Márcio Carvalho
Department of Mechanical Engineering, Pontifícia Universidade Católica do Rio de Janeiro
Rua Marquês de São Vicente, 225, 22451-900. Rio de Janeiro, Brazil
jesus.fernandez@lmmp.mec.puc-rio.br; camorim@lmmp.mec.puc-rio.br; amanda.pessoa@lmmp.mec.puc-rio.br;
jorge@lmmp.mec.puc-rio.br; msc@puc-rio.br

Abstract. *Porous media micromodels have been widely used for pore-scale multiphase flow visualization as they provide a qualitative description of fluid displacement mechanisms through microchannels, constrictions and pores. Besides a refined visualization, the accurate measurement of the pressure drop due exclusively to the porous media is also essential for understanding the physics of fluid mobilization processes. In this research the study of water-oil flow in a PDMS-based porous media micromodel with a random array of straight and constricted microchannels and in-situ pressure drop measurement is presented. Several water-oil injection experiments were performed, monitoring the dynamics of the pressure gradient with coupled transducers, and visualizing the fluid displacement in the porous medium by fluorescence microscopy. The results include steady-state relative permeability curves and non-steady state waterflooding performances. Both oil recovery factors and phase distribution profiles are described based on the operation flow rate, viscosity ratio and surface wettability. Direct observation of the fluid mobilization phenomena at the pore scale improved the physical understanding of the capillary and viscous effects associated with the flow of water and oil in a simple and well-characterized micromodel. This approach opens new opportunities to systematically study pore scale processes in more complex porous networks and fluid systems.*

Keywords: *porous media, micromodels, flow of water and oil, relative permeability, microfluidics.*

1. INTRODUCTION

Multiphase fluid transport through porous structures is a widely studied topic in many industrial and environmental applications. Displacement processes involving immiscible fluids in porous media are crucial to many technological applications, especially in the petroleum industry, including CO_2 sequestration and oil recovery. Two-phase flow in porous medium is usually described by macroscopic laws. However, when capillary forces become important, such laws are not able to account for microscopic effects. Macroscopic multiphase phenomena can only be fully understood through a fundamental comprehension of the complex mechanisms at the pore-scale (Avendaño *et al.*, 2019).

Microfluidic devices have been used to quantify the pore-scale physics in order to relate macroscopic transport properties to microscopic displacement mechanisms. Porous media analogs, known as micromodels, provide a transparent interconnected porous network, which enables the direct visualization of the fluid flow dynamics occurring at the pore level (Anbari *et al.*, 2018; Gunda *et al.*, 2011). Furthermore, when these devices are coupled with precise pressure drop measurements through the porous network, the additional information gathered could lead to important advances in this area.

In immiscible displacement processes in porous media there is no capillary equilibrium in the system and the relative saturation of the fluids is a function of time. The pressure difference between the two sides of a meniscus at any point is equal to the capillary pressure given by Laplace's equation $P_c = 2\gamma cos\theta/r$, where γ is the interfacial tension, θ is the contact angle, and r is the radius of the capillary. The dynamic of two-phase displacement with both capillary and viscous effects can be characterized by two dimensionless numbers: the capillary number $Ca = \mu v/\gamma$, which is the ratio of viscous to capillary forces, and the viscosity ratio $M = \mu_2/\mu_1$, which is the ratio between the viscosity of the displacing

and the displaced fluids. Here, μ and v are respectively the viscosity and average velocity, and the subscripts 1 and 2 refer to the displaced and displacing fluids, respectively.

Depending upon the capillary number and the viscosity ratio, the flow can occur in three different regimes: stable displacement, capillary fingering, and viscous fingering (Lenormand *et al.*, 1988). The displacement behaves differently depending on the relative magnitude of the viscosity ratio. When a more viscous fluid is injected ($M > 1$), the pressure drop in the front is associated to the invading phase, occupying a percolation-like cluster. In unfavorable viscosity ratio ($M < 1$), the pressure drop is associated to the displaced phase, leading to capillary-viscous fingering (Xu *et al.*, 1998). At high Ca, the displacement is stabilized by viscous effects and the flood front is approximately flat. In the fingering regimes, the flood front has many fingers. When fingering is seen in low Ca displacements, it is called capillary fingering. Fingering in high Ca and unfavorable viscosity ratio displacements is called viscous fingering (Lenormand *et al.*, 1988).

Commonly, studies evaluating the efficiency of oil displacement and measuring relative permeability in porous media are characterized with drainage and imbibition profiles. Based on surface wettability, the displacement of a wetting fluid by the injection of a non-wetting fluid is called drainage. In the limiting case of capillary-dominated flow, the invasion of the pores is controlled by the capillary pressure, i.e., the non-wetting fluid must build a threshold pressure difference before it can invade a pore. On the other hand, imbibition is the displacement of a non-wetting fluid by an immiscible wetting fluid, in which pore invasion is favored by the capillary pressure serving as a driving force (Anderson, 1987; Avendaño *et al.*, 2019).

Despite the high theoretical knowledge of the physics behind these microscopic displacement mechanisms, there is still a gap in experimental methodologies that allow, together with the visualization of the fluid-fluid displacement at the pore scale, to correlate macroscopic variables, such as pressure drop, capillary number and viscosity ratio with capillary and viscous effects that dominate the microscopic displacement in porous media of certain intergranular morphology and wettability (Honarpour and Mahmood, 1988; Wu *et al.*, 2012; Xu *et al.*, 2014). From these correlations and in terms of practical application at EOR processes, variables such as relative permeability, residual oil saturation, and phase distribution throughout the porous media become crucial for evaluating the efficiency of immiscible water-oil displacements (Taber, 1980; Iglauer *et al.*, 2012; Avendaño *et al.*, 2019).

In this work, a microfluidic approach is used to investigate the water-oil displacement on PDMS micromodels, monitoring the dynamics of the pressure drop with a coupled transducer and visualizing the fluid displacement in the porous media by means of fluorescence microscopy. Both oil recovery factors and steady-state phase distribution profiles are described based on the operation flow rate, viscosity ratio and surface wettability. In addition, measurements of steady-state water-oil relative permeability in the porous media micromodels at different wettability conditions complete the results. Our systematic methodology allowed direct correlation between pore-scale visualizations and pressure drop measurements, improving the physical understanding of the fluid mobilization phenomena in a PDMS micromodel.

2. MATERIALS AND METHODS

2.1 Fluid properties

Experiments were carried out at 22 °C. The viscosity (μ) and interfacial tension (γ_{wo}) of fluids are reported at this temperature. Milli-Q® water (μ_w = 0.9544 cP) was used as the aqueous phase in all experiments. Sodium dodecyl sulfate (SDS) was added (0.41 wt.%) to this aqueous phase for the oil displacement experiments, and will be referred to as the displacing aqueous phase (μ_w = 0.9623 cP). Two mineral oils were used as displaced oleic phases: Drakeol® 7 (μ_{o1} = 20.4 cP) and 500 PS® (μ_{o2} = 229.8 cP). The water-oil interfacial tension of the system with Drakeol® 7 is 3.25 mN/m, and for the system with 500PS® it is 3.58mN/m. Relative permeability measurement was only determined with the lowest viscosity oil, and its interfacial tension with Milli-Q® water is 13.2 mN/m. In this study all visualizations were done by fluorescence microscopy, using Methylene blue at 0.0004 wt.% in the aqueous phases and Oil-Glo® 33 at 0.1 (v/v)% in the oleic phases.

2.2 Micromodel design and fabrication

Porous media micromodels consist in polydimethylsiloxane (PDMS) channels bonded to a glass surface. First, the capillary network was designed using AutoCAD, as illustrated in Fig. 1. This capillary network is composed of a repetitive 3mm x 3mm cell of 10 x 10 connected channel arrangement of straight and constricted microcapillaries. All the channels have square profile of approximately 100 μm depth x 100 μm width apart from two pore constriction sizes (45 μm and 75 μm) that are randomly distributed.

From the design, a plastic photomask was printed and the micromodel mold was fabricated using standard soft lithography technique (Xia and Whitesides, 1998; McDonald and Whitesides, 2002). The porous media design was patterned on a silicon wafer to produce a 100-μm thick mold. Moreover, PDMS (Sylgard 184 Elastomer Kit, Dow Corning) was mixed with the curing agent at a 10:1 polymer/cross-linker ratio and placed under vacuum. After degassing, PDMS was poured onto the silicon mold and cured inside an oven at 80 °C for 2h. Patterned PDMS was peeled off from the mold

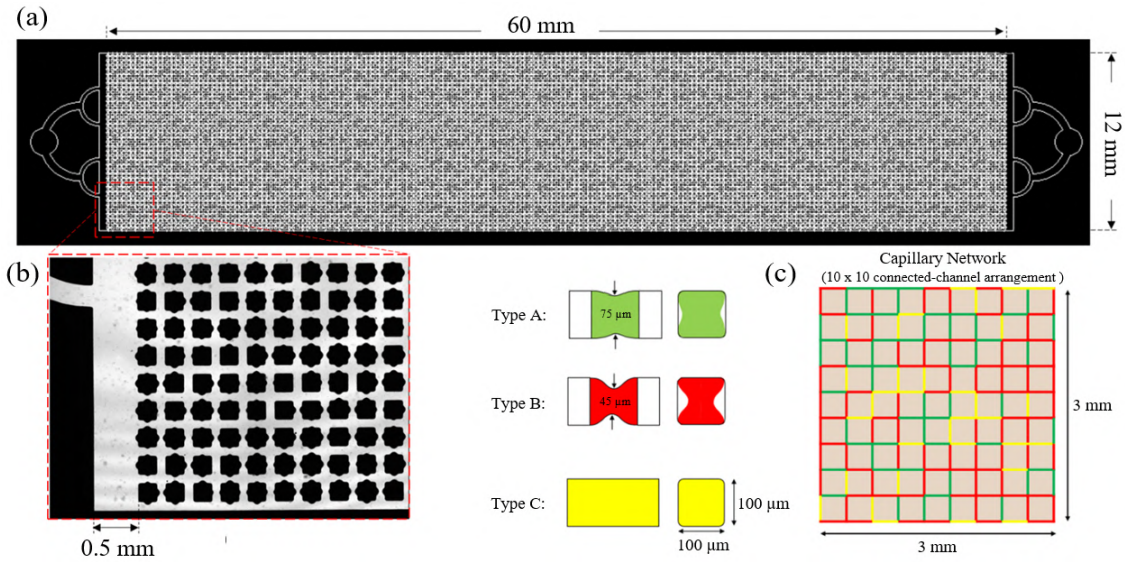

Figure 1. Details of the PDMS-based 2D porous media micromodel. (a) Porous media design. (b) Zooming in on the injection zone and constrictions. (c) Dimensions of the capillary network cell.

and was finally irreversibly bonded to a microscope glass slide through oxygen plasma treatment (0.5 Torr, 30W, 2 min) using a plasma cleaner (PDC-001, Harrick Plasma, USA).

2.3 Wettability alteration

PDMS is hydrophobic (water contact angle $> 90°$), while glass is naturally hydrophilic (water contact angle $\sim 29°$) (Bhattacharya *et al.*, 2005). Thus, each channel in the porous media is composed of three lipophilic walls on a hydrophilic base, which makes the fabricated micromodels be considered as hybrid-wet (HW). The oxygen plasma treatment performed to bond PDMS/Glass renders the PDMS walls water-wet during the first 8 hours, but after 72 hours its lipophilic nature is completely recovered (Bacharouche *et al.*, 2013). In this study, two types of porous media micromodels based on wettability were used: water-wet (WW) when used within one to five hours of bonding and hybrid-wet (HW) when used after 72 hours.

2.4 Micromodel geometric characterization: dimensions, porosity and channel-size distribution

In a SP8 confocal microscope (Leica Microsystems), the fluorescence microscopy technique was used to visualize the porous media in both 2D and 3D. By flooding the micromodel with a 0.01M rhodamine B solution, it was possible to obtain a fluorescence intensity profile along the z-axis, which represents the microchannel cross-sectional height (H). By image processing, both the size distribution of channels and constrictions throughout the entire porous medium and the 2D-projection of the pore volume were measured. This projection, referred to as the porous area (A_P), allowed with the channel height to determine the internal volume of the porous space (V_P). In addition, from the 2D total area covered by the porous media (A_T), the area-based micromodel porosity (ϕ) was calculated as $\phi = A_P/A_T$.

2.5 Single-phase flow experiments: Absolute permeability measurement

Based on single-phase Darcy's Law Eq. (1), the absolute permeability (K_{abs}) of the micromodel was calculated from measured values of pressure drop across the porous media (ΔP) during the flow of Milli-Q® water at different flow rates (Q). The experiments were conducted as follows: initially (i) the micromodel was flooded with CO_2 by flow at 0.1 bar, then (ii) the micromodel was flooded with the aqueous phase from a single-syringe pump (model Harvard Apparatus Elite 11) connected to the micromodel inlet port by 250 μm ID tubing. Finally, (iii) at the steady state of each injection flow rate (from 1 to 16 ml/h), the pressure drop across the porous media was measured using two pressure transducers (Velki, 15 psi and WIKA, 1.5 psi) connected directly at the inlet and outlet boundaries of the porous medium by 800 μm ID tubing. The absolute permeability was calculated from the average of three independent experiments.

$$K_{abs} = \frac{L}{A}\mu\frac{Q}{\Delta P} \tag{1}$$

where L is the micromodel length, A is the micromodel cross-sectional area and μ is the fluid viscosity.

2.6 Two-phase flow experiments: Relative permeability measurements

Two types of experiments involving both water and oil flow were performed: at transient-state and at steady-state conditions. In the transient-state experiments, a single waterflooding was performed on WW and HW micromodels initially saturated with one of the oleic phases. The water-oil immiscible displacement was analyzed at two injection flow rates (Q_1 = 0.5 and Q_2 = 5 ml/h), two viscosity ratios ($\mu_w/\mu_{o1} \sim 0.05$ and $\mu_w/\mu_{o2} \sim 0.004$) and for the aqueous phase with and without surfactant (SDS). During the flooding, the pressure drop across the porous media was measured and, after the injection of 10 pore volumes (PV) of the displacing phase, which ensured the steady-state flow condition, the injection was stopped. A complete image of the micromodel was acquired to observe the distribution of the phases and to quantify the remaining saturation of the oleic phase (S_O) by subsequent image processing. S_O is defined as the fraction of the porous area occupied by the oleic phase after waterflooding.

The second type of experiment was designed to measure the steady-state relative permeability curves of the aqueous phase without surfactant and the oleic phase with lower viscosity in both the WW and HW micromodels. The porous media was initially saturated with the oleic phase and then, at a constant total flow rate of 2 ml/h (Q_T), both phases were injected simultaneously. In each run, the flow rates of the aqueous phase (Q_W) and the oleic phase (Q_O) were set at a certain proportion between them (proportion referred to the aqueous phase and named as f-value, $f = Q_W/Q_T$). Thus, the f-value was swept from 0 (injection of oil) to 1, which corresponds to the end point of the experiment in which only the aqueous phase was injected. At each steady-state condition, indicated by a constant value of pressure drop, the injection was stopped and a complete image of the micromodel was acquired.

Based on the multiphase extension of Darcy's Law Eq. (2), the effective permeability of each phase ($K_{eff,i}$) was calculated from the injection flow rate of this phase (Q_i) and the steady-state pressure drop (ΔP). The relative permeability corresponds to the ratio between the effective permeability and the absolute permeability of the porous media (K_{abs}). Each f-value defines the relative permeability of the aqueous (K_{rw}) and oleic (K_{ro}) phases at a specific condition of relative saturation. The relative saturation of the aqueous phase (S_W) was calculated by image processing and is defined as the fraction of the porous area occupied by the aqueous phase at the steady state.

$$K_{eff,i} = \frac{L}{A}\mu_i \frac{Q_i}{\Delta P} \tag{2}$$

where the subscript i refers to the phase i.

2.7 Image processing

An 8-bit full image of the micromodel was acquired in all tests performed. These images are composed of two channels corresponding to the detection of the aqueous phase (cyan in color) and the oleic phase (yellow in color). Image processing was carried out using ImageJ® software, and the porous area occupied by each phase was measured.

3. RESULTS

3.1 Micromodel characterization

The 2D porous media is (57.7 $\pm$ 0.1) mm long, (11.4 $\pm$ 0.1) mm wide and its average height is (99 $\pm$ 6) μm. The area-based micromodel porosity (ϕ) resulted in 0.54 and, from the average height, the internal volume of the porous media was calculated in $V_P \sim 36$ μL. Figure 2 shows the actual distribution of straight and constricted microchannel sizes throughout the porous media, exhibiting modal sizes of 47.8 μm, 75.6 μm and 98.1 μm.

From the pressure drop measurement in single-phase flooding experiments, it was observed that the order of magnitude of the pressure drop in the internal inlet and outlet connections of the porous media micromodel is as important as that due exclusively to the porous space. Therefore, we investigated two distinct sites for pressure drop measurement: (i) outside the porous medium (ΔP_{opm}), that is, at the inlet and outlet of the micromodel, and (ii) inside the porous medium (ΔP_{ipm}) which is measured at the borders of the porous media matrix.

Figure 3a shows the pressure drop (ΔP) versus the flow rate of Milli-Q® water (Q) flooding the micromodel. Figure 3b shows the calculations from Darcy's Law, in which the absolute permeability is obtained directly from the slope. In a first approximation, when the pressure drop is measured outside the porous media, ΔP_{opm} exhibits higher values, suggesting a micromodel permeability of 43.5 D (Fig. 3b, dotted gray line). However, when the pressure drop is measured at the borders of the porous media (ΔP_{ipm}), a significant reduction in the measured values of ΔP is observed, which is expected since the head loss due to the effect of the bifurcated inlet and outlet channels that connect the porous media are not include in the measurement. From this methodology, we can estimate the real permeability of the porous media micromodel as (105.3 $\pm$ 0.2) D (Fig. 3b, continuous black line).

These results demonstrate the importance of measuring the pressure drop directly inside the porous media. This methodology was adopted in all the experiments that will be presented from here on.

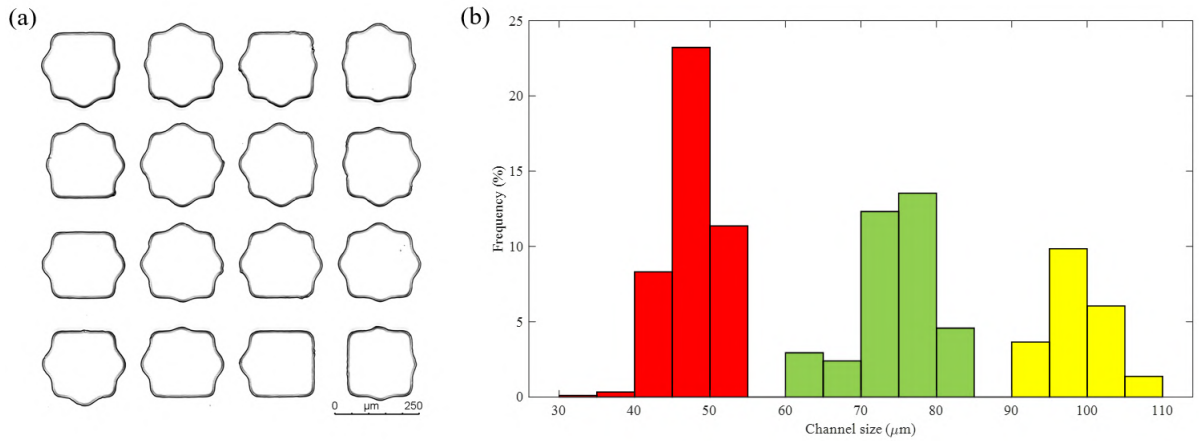

Figure 2. (a) Micrograph of straight and constricted PDMS/glass channels. (b) Size distribution of channels in the porous media micromodel.

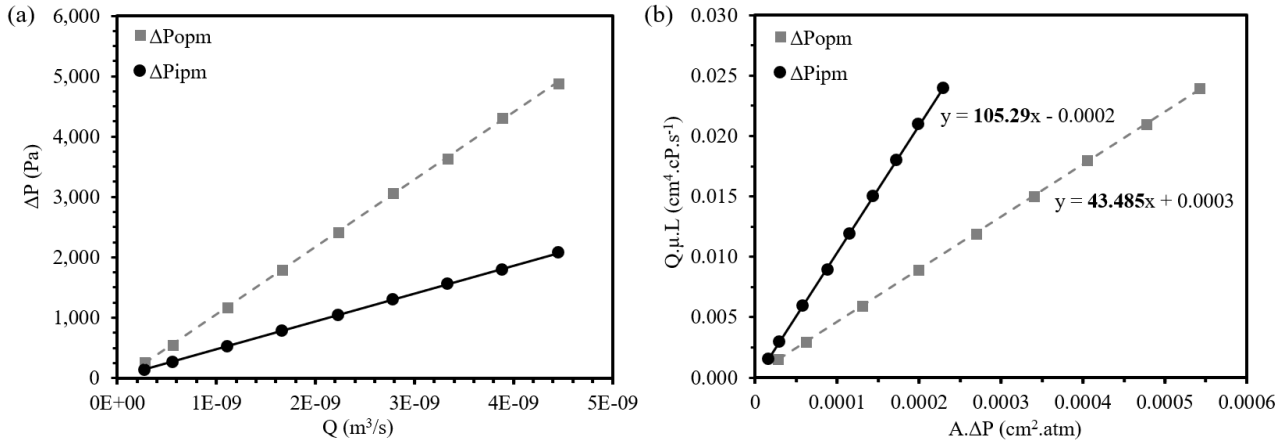

Figure 3. PDMS porous media micromodel absolute permeability (K_{abs}). (a) Pressure drop measurements (ΔP) against water flow rate (Q). (b) Calculations based on Darcy's Law, which provides K_{abs} directly from the slope.

3.2 Non-steady state experiments: waterflooding performance

It is well documented that the performance of a waterflooding depends on the wettability of the porous medium, the fluid-fluid interfacial tension, the operating flow rate and the viscosity ratio between the phases. Several experiments for different combinations of these variables were performed in the PDMS porous media micromodels and are presented below. The results are composed of the transient pressure gradient profile during each test and the respective distribution of the phases inside the porous media at the steady-state final condition (Fig. 4 to Fig. 6). It is important to highlight that no mechanical filtering or material accumulation of the oleic phase was observed throughout the experiments, since the fluids were immiscible and non-reactive. In that regard, the steady state distribution of the phases in the porous media corresponds to the displacing aqueous phase in equilibrium with the residual oleic phase.

3.2.1 Injection flow rate effect

The displacement of the more-viscous oleic phase ($\mu_w/\mu_{o2} \sim 0.004$) at two injection flow rates (Q_1 = 0.5 and Q_2 = 5 ml/h) in the water-wet (WW) device is presented in Fig. 4. At both flow rates, the pressure gradient follows the same increasing trend, as expected. Figure 4b and Figure 4c show that, at the steady-state condition, the flooding performed at Q_2 = 5 ml/h delivers more oil than the one at Q_1 = 0.5 ml/h. The remaining oil saturation in the porous media resulted in 59.9% and 33.2%, respectively. All these observations allow us to argue that in the viscosity ratio studied, viscous forces macroscopically dominate the transport mechanisms for oil recovery.

3.2.2 Water-oil viscosity ratio effect

Now the effect of the viscosity ratio (μ_w/μ_o) on the displacement of an oleic phase by flooding with the displacing aqueous phase at Q_1 = 0.5 ml/h in the water-wet device (WW) is presented. Figure 5a shows that the pressure gradient is

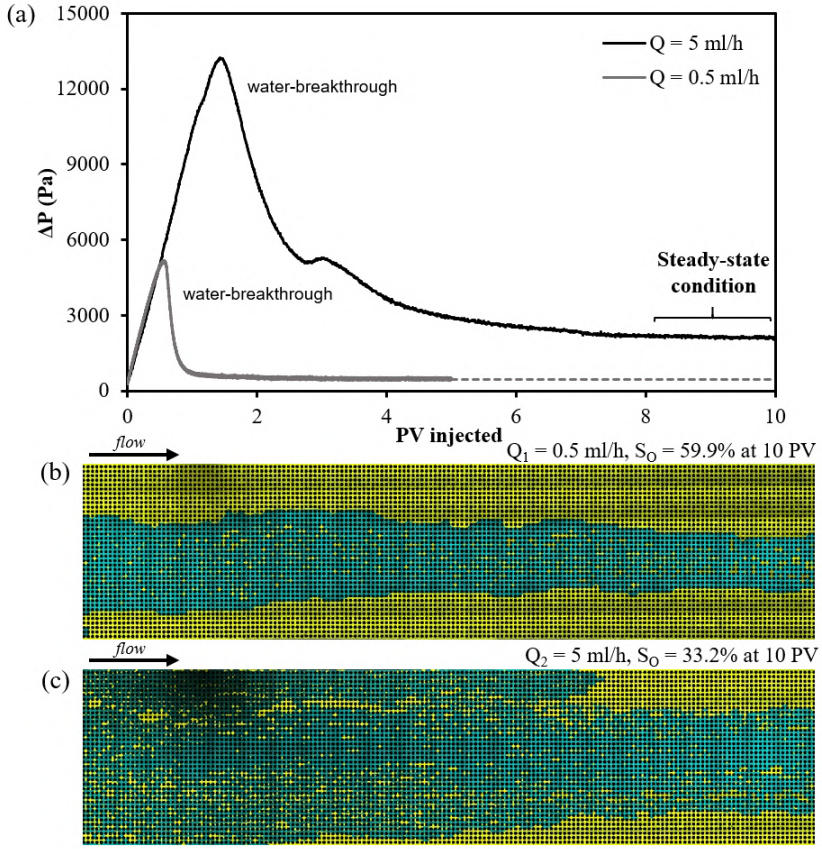

Figure 4. Effect of injection flow rate in the WW device. (a) Pressure drop through the porous media during waterflooding. Micrographs taken at steady-state at (b) Q_1 = 0.5 ml/h (S_O = 59.9%) and (c) Q_2 = 5 ml/h (S_O = 33.2%). Aqueous phase (SDS 0.41 wt.%) dyed in cyan and higher-viscosity oleic phase ($\mu_w/\mu_{o2} \sim 0.004$) dyed in yellow.

greater in the porous media occupied by the more-viscous oleic phase ($\mu_w/\mu_{o2} \sim 0.004$), which offers the most unfavorable condition for its mobilization. In addition, it is observed that the growth of the pressure gradient during invasion of water into the porous media is more accelerated when the viscosity ratio between the phases is greater ($\mu_w/\mu_{o1} \sim 0.05$), leading to an earlier water breakthrough. Despite this, due to lower viscous forces in this case, Fig. 5b shows that the central flow path with high saturation of water that is created in the porous media has much more lateral growth, leading to further reduction in the unswept oil banks.

Although the steady state of both systems is reached at similar PV injected (Fig. 5a), the sweeping efficiency is different, and seems to be associated with post-breakthrough oil mobilization phenomena influenced by a compromise between the viscous and capillary forces. Figure 4b and Figure 5b illustrate the steady-state phase distribution for the two contrasted systems as a function of the viscosity ratio. Oil recovery increased $\sim 50\%$ (based on the total original oil) when the viscosity of the displaced phase is reduced from 229.8 cP (Fig. 4b) to 20.4 cP (Fig. 5b). In this case, the reduction of the viscous forces by modifying the viscosity of the displaced phase, led to more efficient waterflooding.

3.2.3 Porous media wettability effect

Some enhanced oil recovery approaches aim to increase the efficiency of the displacement front in waterflooding operations by regulating the viscous effect and the capillary effect. As seen before, for a given porous matrix (that is, the porous media micromodel), the viscous effect seems to be directly related to the injection flow rate and the viscosity ratio between the phases. The capillary effect, as has been widely reported, seems to depend on the wettability of the porous matrix and the fluid-fluid interfacial tension (Xu *et al.*, 2014; Wu *et al.*, 2012).

In this section, the effect of wettability on oil displacement was analyzed with a system in which the capillary effect was strongly favored over the viscous effect. The waterflooding was performed at a very low injection flow rate (Q_3 = 0.2 ml/h) with the aqueous phase without surfactant (without SDS) and using the lower-viscosity oleic phase ($\mu_w/\mu_{o1} \sim 0.05$) in both WW and HW micromodels.

Based on the dynamics of the pressure gradient during the flooding (Fig. 6a), the sequence of events up to the steady state condition (Fig. 6b and Fig. 6c) can be summarize as follows: at the first moments of the aqueous phase invasion into the porous media, a pressure threshold in both wettability conditions suggests a compromise between the viscous

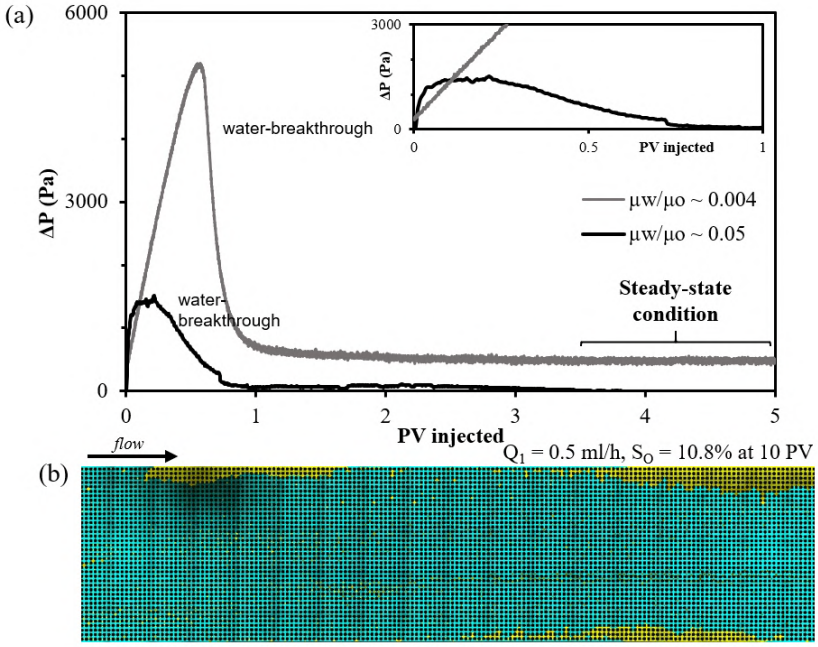

Figure 5. Effect of water-oil viscosity ratio at Q_1 = 0.5 ml/h. (a) Pressure drop through the porous media during water-flooding for oleic phases of $\mu_w/\mu_o \sim 0.004$ and 0.05. (b) Micrograph taken at steady-state (S_O = 10.8%). Aqueous phase (SDS 0.41 wt.%) dyed in cyan and lower-viscosity oleic phase ($\mu_w/\mu_{o1} \sim 0.05$) dyed in yellow.

resistance to move the oil and the capillary forces that can help (in the WW device) or oppose (in the HW device) to the flow of water. For about 0.25 PV injected, the pressure gradient slightly decreases but its value is still comparable to that of the first threshold. In the WW micromodel, the aqueous phase flowed through a wide channel of high saturation in the main direction of flow, leaving lateral banks of unswept oil. While, in the HW micromodel, lateral flow of the aqueous phase swept more uniformly across the porous media, leaving a large number of small oil islands.

Once the aqueous phase circulates through continuous pathways from the inlet to the outlet of the micromodel, the pressure gradient dropped by approximately 66% in both the WW and HW porous media. After the water breakthrough, the steady-state condition in the WW micromodel was quickly reached, so that, there was no longer access to the unswept oil parts and the oil saturation remained at 24.8% (Fig. 6b). Instead, in the HW micromodel, the steady-state condition was delayed by additional mobilization of oil during almost two more PV injected and, at the end, the remaining oil saturation was 15.1% (Fig. 6c). This increase in the recovered oil when the porous medium has lipophilic character agrees with some previously reported experimental evidence from porous media micromodels (Avendaño *et al.*, 2019).

3.3 Steady-state experiments: relative permeability measurement

A next point of interest in this study was the analysis of the steady-state simultaneous flow of water and oil through the WW and HW porous media micromodels. As a base system, the one presented in Sec. 3.2.3 – lower-viscosity oleic phase ($\mu_w/\mu_{o1} \sim 0.05$) and higher fluid-fluid interfacial tension – was chosen. This selection is intended to preserve the effect of both viscous and capillary forces during the two-phase flow. Figure 7 shows the relative permeability of the phases at different water saturations (S_W) of the porous media.

At first sight, the locus described by the relative permeability curves follows a trend like that widely described in literature for water and oil flow through homogeneous porous media (Honarpour and Mahmood, 1988; Moghadasi *et al.*, 2016). However, based on wettability, the behavior conflicts with the conventional wisdom that relative permeability of water decreases and relative permeability of oil increases as the system becomes more water-wet (Anderson, 1987). In this case, it was found that when the oil-wet PDMS channel walls become water-wet, the relative permeability of water (K_{rw}) is slightly altered at low water saturations and the relative permeability of oil (K_{ro}) is decreased more rapidly as water saturation increases, leading to a higher remaining oil saturation. These observations are consistent with those found in the non-steady state experiments performed with the same system, in which the remaining oil saturation was higher in the WW device (Fig. 6b).

The steady-state relative permeability behavior is a function not only of the relative saturation, but also of the way water and oil are distributed throughout the porous medium. Both the relative saturation and the fluid distribution depend directly on the injection flow ratio (f-value) and the surface wettability. Then, once the volume of water and oil occupying the pore space reaches the steady state, the full cocurrent flow that is injected at one port is produced at the other, leading

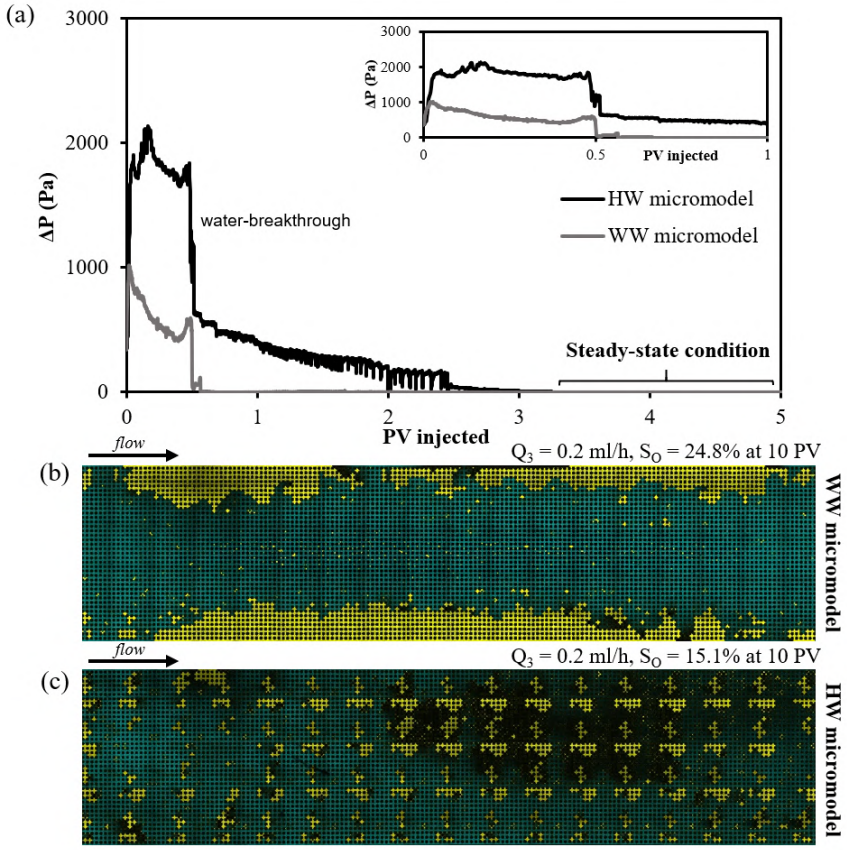

Figure 6. Effect of porous media wettability at Q_3 = 0.2 ml/h. (a) Pressure drop through the porous media during waterflooding. Micrographs taken at steady-state using (b) WW (S_O = 24.8%) and (c) HW (S_O = 15.1%) micromodels. Aqueous phase (Milli-Q® water) dyed in cyan and lower-viscosity oleic phase ($\mu_w/\mu_{o1} \sim 0.05$) dyed in yellow.

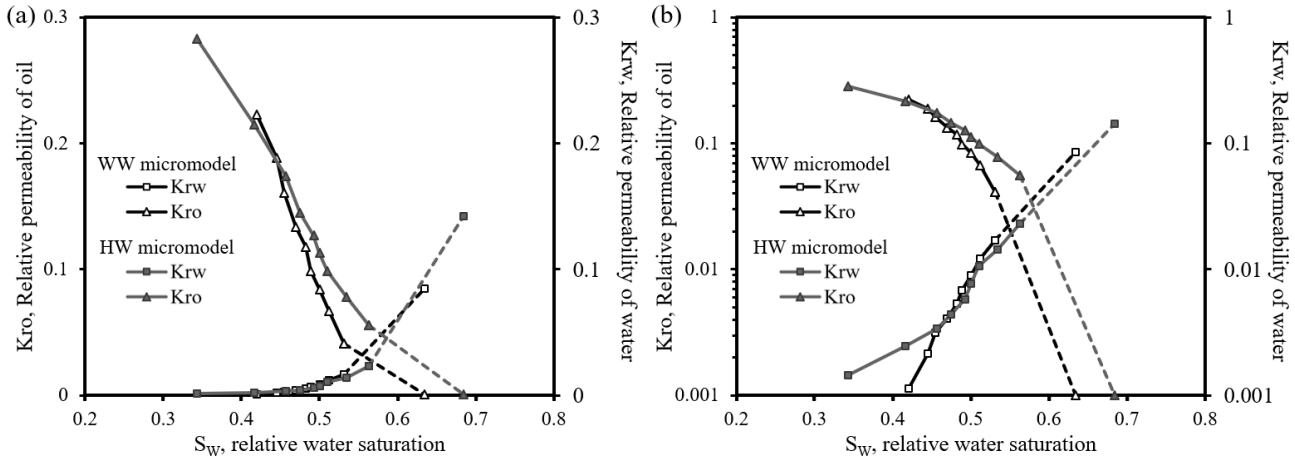

Figure 7. Steady-state relative permeability of water (K_{rw}) and oil (K_{ro}) at different water saturations (S_W) in the water-wet (WW) and hybrid-wet (HW) porous media micromodels.

to a stable pressure drop and phase saturation across the porous media micromodel.

When analyzing the first and last point of the relative permeability curves and the microphotographs of the porous media at these steady-state conditions, it is observed that in the first point (f-value = 0.1, Fig. 8a) the greatest water retention occurs in the WW micromodel as loosely connected fluid units attached to hydrophilic walls. At the other extreme, which corresponds to the injection of only aqueous phase (f-value = 1, Fig. 8b), the greatest saturation of water is verified in the HW micromodel and comes as more connected water pathways that were able to transport and deliver more oil. In both wettability conditions, the snap-off phenomenon is identified for the aqueous phase in the WW micromodel (Fig. 8a) and for the oleic phase in the HW micromodel (Fig. 8b).

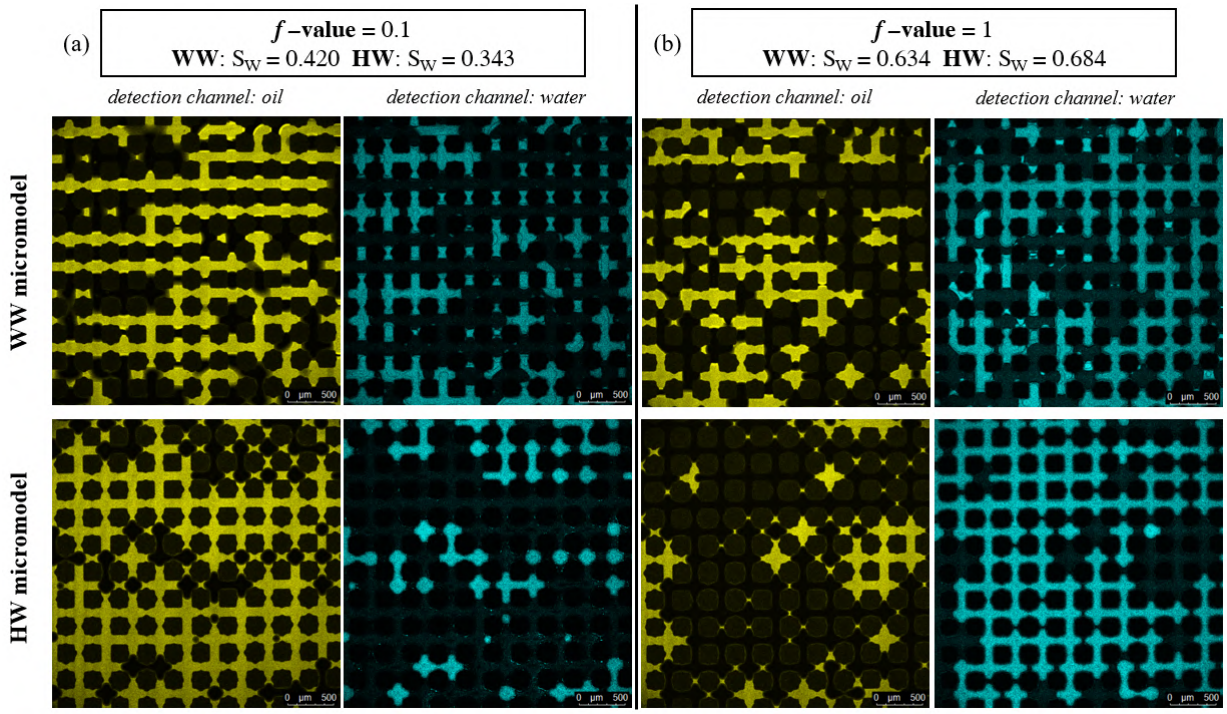

Figure 8. Micrographs taken during simultaneous-flow of water and oil through WW and HW micromodels. Two different proportions of water in the total flow ($f = Q_W/Q_T$) are shown: f-value of (a) 0.1 and (b) 1. Aqueous phase (Milli-Q® water) dyed in cyan and lower-viscosity oleic phase ($\mu_w/\mu_{o1} \sim$ 0.05) dyed in yellow.

Based on capillary forces, during the water-oil displacement there should be a drive effect for the wetting phase, while there should be a resistance effect for the non-wetting phase. The reduced permeability of the oleic phase in the WW micromodel suggests that although this phase flows through non-wetted channels, capillary forces could be creating a greater resistance to flow and, consequently, a higher oil retention as the saturation of water in the porous medium increases. In the HW micromodel, although the oleic phase wets the PDMS walls, favorable capillary forces may help this less-connected phase to flow more easily through the porous media with high water saturation. Regarding the aqueous phase, it is interesting to note that, initially, the occupancy in the WW micromodel is higher (Fig. 8a), but it is not as permeable as in the HW micromodel when compared at the same saturation (for $S_W < 0.455$ in Fig. 7b). Then, as the water saturation increases and therefore its connectivity in the porous medium, K_{rw} increases following the same trend in both the HW and WW micromodels.

4. CONCLUSIONS

Steady-state relative permeability maps of water and oil were accurately determined in a 2D microfluidic porous media device as a function of water saturation and surface wettability. Our comprehensive methodology for pore-scale visualization and accurate measurement of pressure drop in single- and two-phase flow experiments made possible to evaluate the effect of water injection flow rate, water-oil viscosity ratio and porous matrix wettability on oil recovery factors and phase distribution profiles.

In water-wet micromodels, it was found that by decreasing the water injection flow rate or increasing the oil viscosity, the total oil recovery is greater. In addition, by increasing the porous medium's lipophilic character, more oil is displaced, due to the favored lateral flow of water and some mobilization phenomena after breakthrough.

More importantly, the steady-state relative permeability of water and oil showed that pore occupancy at this condition is sensitive to changes in wettability, leading to a clear identification of the snap-off phenomenon. The relative permeability of oil was increased in the more lipophilic porous medium, which suggests that favorable capillary forces help oil to flow easily. This approach opens new opportunities to systematically study pore scale processes in more complex porous networks and fluid systems.

5. ACKNOWLEDGEMENTS

The authors acknowledge the financial support from the Coordination for the Improvement of Higher Education Personnel (CAPES), the National Council for Scientific and Technological Development (CNPq), Repsol Sinopec of Brazil and the National Agency of Petroleum, Natural Gas and Biofuels (ANP).

6. REFERENCES

Anbari, A., Chien, H.T., Datta, S.S., Deng, W., Weitz, D.A. and Fan, J., 2018. "Microfluidic model porous media: Fabrication and applications". *Small*, Vol. 14, No. 18, p. 1703575.

Anderson, W.G., 1987. "Wettability Literature Survey Part 5: The Effects of Wettability on Relative Permeability". *Journal of Petroleum Technology*, Vol. 39, No. 11, pp. 1453–1468. ISSN 0149-2136.

Avendaño, J., Lima, N., Quevedo, A. and Carvalho, M., 2019. "Effect of surface wettability on immiscible displacement in a microfluidic porous media". *Energies*, Vol. 12, No. 4. ISSN 1996-1073.

Bacharouche, J., Haidara, H., Kunemann, P., Vallat, M.F. and Roucoules, V., 2013. "Singularities in hydrophobic recovery of plasma treated polydimethylsiloxane surfaces under non-contaminant atmosphere". *Sensors and Actuators A: Physical*, Vol. 197, pp. 25–29. ISSN 0924-4247.

Bhattacharya, S., Datta, A., Berg, J. and Gangopadhyay, S., 2005. "Studies on surface wettability of poly(dimethyl) siloxane (pdms) and glass under oxygen-plasma treatment and correlation with bond strength". *Journal of Microelectromechanical Systems*, Vol. 14, No. 3, pp. 590–597.

Gunda, N.S.K., Bera, B., Karadimitriou, N.K., Mitra, S.K. and Hassanizadeh, S.M., 2011. "Reservoir-on-a-chip (roc): A new paradigm in reservoir engineering". *Lab on a Chip*, Vol. 11, No. 22, pp. 3785–3792.

Honarpour, M. and Mahmood, S., 1988. "Relative-Permeability Measurements: An Overview". *Journal of Petroleum Technology*, Vol. 40, No. 08, pp. 963–966.

Iglauer, S., Fernø, M., Shearing, P. and Blunt, M., 2012. "Comparison of residual oil cluster size distribution, morphology and saturation in oil-wet and water-wet sandstone". *Journal of Colloid and Interface Science*, Vol. 375, No. 1, pp. 187–192. ISSN 0021-9797.

Lenormand, R., Touboul, E. and Zarcone, C., 1988. "Numerical models and experiments on immiscible displacements in porous media". *Journal of fluid mechanics*, Vol. 189, pp. 165–187.

McDonald, J.C. and Whitesides, G.M., 2002. "Poly(dimethylsiloxane) as a material for fabricating microfluidic devices". *Accounts of Chemical Research*, Vol. 35, No. 7, pp. 491–499.

Moghadasi, L., Guadagnini, A., Inzoli, F., Bartosek, M. and Renna, D., 2016. "Characterization of two- and three-phase relative permeability of water-wet porous media through x-ray saturation measurements". *Journal of Petroleum Science and Engineering*, Vol. 145, pp. 453–463. ISSN 0920-4105.

Taber, J.J., 1980. "Research on enhanced oil recovery: past, present and future". *Pure and Applied Chemistry*, Vol. 52, No. 5, pp. 1323–1347.

Wu, M., Xiao, F., Johnson-Paben, R., Retterer, S.T., Yin, X. and Neeves, K.B., 2012. "Single- and two-phase flow in microfluidic porous media analogs based on voronoi tessellation". Vol. 12, No. 2. ISSN 1473–0197.

Xia, Y. and Whitesides, G.M., 1998. "Soft lithography". *Annual Review of Materials Science*, Vol. 28, No. 1, pp. 153–184.

Xu, B., Yortsos, Y. and Salin, D., 1998. "Invasion percolation with viscous forces". *Physical Review E*, Vol. 57, No. 1, p. 739.

Xu, W., Ok, J.T., Xiao, F., Neeves, K.B. and Yin, X., 2014. "Effect of pore geometry and interfacial tension on water-oil displacement efficiency in oil-wet microfluidic porous media analogs". *Physics of Fluids*, Vol. 26, No. 9, p. 093102.

7. RESPONSIBILITY NOTICE

The authors are solely responsible for the printed material included in this paper.